VNUHCM Journal of Science and Technology Development 2026, 29(3):4271-4282

Open Access Full Text Article

Research Article

Influence of Bi0.5Na0.5HfO3 Content on Structural Phase Transitions and Electrical Properties of (1−x)(Li0.04K0.48Na0.48)(Nb0.95Sb0.05)O3-xBi0.5Na0.5HfO3 Ceramics

Le Dai Vuong[1,*], Vo Quang Nha[1], Huynh Thi Thuy Linh[1], Vo Thi Thanh Kieu[2], Vo Thanh Tung[3], Le Van Tan[3,4,5,*]

Use your smartphone to scan this QR code and download this article

ABSTRACT

Lead-free $(1-x)(Li_{0.04}K_{0.48}Na_{0.48})(Nb_{0.95}Sb_{0.05})O_3$ (LKNNS)–$xBi_{0.5}Na_{0.5}HfO_3$ (BNH) ceramics ($x = 0$–0.035) were synthesized via a conventional solid-state route combined with a two-step sintering process to tailor their phase configurations and functional properties. The effects of BNH content on the structural evolution, microstructure, and electrical properties of LKNNS-based ceramics were systematically investigated. Structural analysis revealed a composition-driven transition from predominantly orthorhombic symmetry (*Amm2*) toward a rhombohedral (*R3m*) structure, passing through an intermediate tetragonal–rhombohedral multiphase region. The formation of this multiphase region significantly enhanced the dielectric and piezoelectric responses of the ceramics. The composition containing 0.025 mol BNH (0.975LKNNS–0.025BNH) delivered the best overall electrical performance. This sample exhibited elevated electromechanical coupling coefficients ($k = 0.37$; $k_t = 0.39$), an improved piezoelectric response ($d_{33} = 230$ pC/N), and enhanced dielectric permittivity ($\varepsilon_r = 1137$, $e_{max} = 6274$). Additionally, a high remnant polarization ($_r = 15.6$ μC/cm^2) was achieved at $x = 0.015$. With increasing BNH content, the Curie temperature (T_C) decreased gradually from 364 to 318 °C, while T_{O-T} decreased from 110 to 60 °C. Meanwhile, the diffuseness parameter (γ) slightly increased from 1.34 to 1.56, suggesting that the relaxor characteristics increased with BNH content owing to structural disorder within the ABO_3 perovskite structure. These findings indicate that LKNNS–BNH ceramics are highly promising candidates for environmentally friendly piezoelectric and power-related applications.

Key words: LKNNS–BNH, Two-step sintering, R–O phase boundary, Energy coefficient

[1]*School of Engineering and Technology - Hue University, Hue City, Vietnam*

[2]*Hue Industrial College, Hue City, Vietnam*

[3]*University of Sciences, Hue University, Hue City, Vietnam*

[4]*Laboratory of Applied Physics, Science and Technology Advanced Institute, Van Lang University, Ho Chi Minh City, Vietnam*

[5]*Faculty of Applied Technology, Van Lang School of Technology, Van Lang University, Ho Chi Minh City, Vietnam*

Correspondence

Le Dai Vuong, School of Engineering and Technology - Hue University, Hue City, Vietnam

Email: ldvuong@hueuni.edu.vn

Correspondence

Le Van Tan, University of Sciences, Hue University, Hue City, Vietnam

Laboratory of Applied Physics, Science and Technology Advanced Institute, Van Lang University, Ho Chi Minh City, Vietnam

Faculty of Applied Technology, Van Lang School of Technology, Van Lang University, Ho Chi Minh City, Vietnam

Email: levantan@vlu.edu.vn

INTRODUCTION

For six decades, $Pb(Zr_{1-x}Ti_x)O_3$-based piezoelectric materials have been extensively investigated and successfully applied in a broad range of devices, including capacitors, high-density memory systems, low-, medium-, and high-power ultrasonic transducers, for medical, biological, chemical, and pharmaceutical applications. Additionally, these materials are widely used in piezoelectric transformers owing to their effective combination of dielectric permittivity, ferroelectric polarization characteristics, and electromechanical response[1–3]. Nevertheless, growing environmental regulations and health concerns related to lead toxicity have accelerated the development of environmentally benign alternatives. Consequently, several lead-free systems, including $Bi_{0.5}(Na_x\ K_{1-x})TiO_3$-, $BaTiO_3$-, and $(K_{1-y}\ Na_y)NbO_3$ (KNN)-based ceramics, have been proposed[4–6].

KNN-derived ceramics are regarded as one of the most viable lead-free systems, primarily because they combine a strong piezoelectric response with a comparatively high Curie temperature (T_C), enabling their use in practical engineering applications[7–9]. Recently, the functional properties of KNN ceramics have been enhanced by tailoring the room-temperature rhombohedral–tetragonal (R–T) phase boundary through compositional modification. The incorporation of perovskite additives, such as $Bi_{0.5}K_{0.5}HfO_3$, $Bi_{0.5}Na_{0.5}HfO_3$, $CaZrO_3$, $BaZrO_3$,and $BaTiO_3$, enables simultaneous adjustment of the rhombohedral–orthorhombic (R–O) and orthorhombic–tetragonal (O–T) transition temperatures (T_{R-O} and T_{O-T}) toward ambient conditions, leading to significant improvements in piezoelectric performance[10,11]. Previous investigations have also confirmed the beneficial role of BNH in constructing multiphase boundaries within KNN-based ceramics. Zhang et al.[12] introduced 4.5 mol% BNH into KNNS

Cite this article : Vuong L D, Nha V Q, Linh H T T, Kieu V T T, Tung V T, Tan L V. **Influence of Bi0.5Na0.5HfO3 Content on Structural Phase Transitions and Electrical Properties of (1−x)(Li0.04K0.48Na0.48)(Nb0.95Sb0.05)O3-xBi0.5Na0.5HfO3 Ceramics** . *Sci. Tech. Dev. J.* 2026; 29(3):x-x.

History
- Received: 12-01-2026
- Revised: 16-05-2026
- Accepted: 14-08-2026
- Published Online: 28-09-2026

DOI : https://doi.org/10.32508/vnuhcmj-std.v29i3.4652

and observed a pronounced piezoelectric response (d_{33} = 540 pC/N), which was attributed to the stabilization of an *R*–*O*–*T* coexistence region at ambient temperature. Similarly, Tao et al.[13] showed that compositions containing 3.5 mol% BNH, situated near the *R*– *T* boundary, exhibited enhanced electromechanical performance with a d_{33} of 418 pC/N, planar electromechanical coupling factor k_p of 0.45, and a T_C of 242 °C.

Moreover, our recent research on $(Li_{0.04}K_{0.48}Na_{0.48})(Nb_{0.95}Sb_{0.05})O_3$ (LKNNS) ceramics demonstrated that optimal electrical properties could be achieved via a two-step sintering technique, yielding a k_p of 0.33, an ε_r of 849, a tanδ of 0.073, and a d_{33} of 195 pC/N, resulting in a recoverable energy storage density W_{rec} of 0.36 J/cm^3 and an energy coefficient h of 48.1%[9]. In contrast to previously reported KNN–BNH systems[13], the present work emphasizes the combined effects of lithium (Li) incorporation and a two-step sintering strategy in tailoring the phase boundaries and thereby optimizing the electrical properties. With a low melting point of roughly 181 °C, Li acts as a sintering aid that helps reduce the processing temperature, which facilitates grain rearrangement and densification during sintering. Building on these findings, the present study aims to further enhance the physical properties of (1−*x*)LKNNS– *x*BNH (*x* = 0.0, 0.015, 0.025, and 0.035) ceramics by employing a two-step sintering strategy to establish a new phase boundary at room temperature.

METHODS AND EXPERIMENTS

A series of lead-free (1−*x*)LKNNS– *x*BNH (*x* = 0.0, 0.015, 0.025, and 0.035) ceramics were produced through a conventional solid-state reaction route, followed by a two-step sintering strategy to ensure complete phase formation and densification. High-purity starting powders (purity > 99%) composed of K_2CO_3, Na_2CO_3, Li_2CO_3, Nb_2O_5, Sb_2O_3, Bi_2O_3, and HfO_2 were proportioned according to the nominal compositions and thoroughly mixed via planetary ball milling for 20 h. The resulting powder blend was heat-treated at 850 °C for 2 h to facilitate synthesis of the LKNNS–BNH perovskite phase.

After the initial calcination step, the powders underwent secondary ball milling for 20 h to ensure compositional uniformity. The fine mixture was then uniaxially pressed into disk-shaped compacts under a load of 1.5 T/cm^2 (12 mm diameter, ~2 mm thickness), followed by densification via a controlled two-step thermal treatment[9]. The two-step sintering schedule involved rapid initial heating to 1150 °C with a dwell time of 5 min, followed by controlled cooling to 1050 °C and a subsequent holding period of 4 h. To minimize the volatilization of alkali elements (K, Na, Li), the dwell time at the peak temperature (1150 °C) was strictly limited to 5 min during the first sintering step. These sintering parameters were selected based on optimization protocols established in our previous work[9] to achieve maximum bulk density and a well-controlled microstructure.

Phase identification and microstructural observation of the sintered LKNNS–BNH ceramics were carried out under ambient conditions using X-ray diffraction (XRD) and scanning electron microscopy (SEM). The bulk densities were identified using Archimedes' method. Dielectric properties were characterized using an RLC impedance analyzer over a wide temperature range, and the piezoelectric and ferroelectric properties were evaluated using a piezo-d_{33} meter and a ferroelectric workstation, respectively.

RESULTS AND DISCUSSION

As a fundamental indicator of material quality and essential for subsequent property analysis, the bulk densities of the fabricated ceramics were examined. Generally, ceramics exhibiting a relative density below 90% of the theoretical value are considered insufficiently dense, necessitating modification of the process parameters. As shown in Fig. 1, the bulk density of the (1−*x*)LKNNS–xBNH system exhibits composition-dependent behavior. An increase in *x* initially promotes densification, leading to a peak value of 4.57 g/cm^3 (corresponding to 98.1% relative density) at *x* = 0.025, followed by a reduction at higher substitution levels. The densification enhancement is primarily ascribed to improved crystal growth and a more homogeneous, compact grain arrangement. During sintering, thermal shrinkage plays a dominant role and is strongly influenced by the evolution of the ceramic microstructure[10,11,14]. Typically, measured bulk densities fall within the range of 4.41–4.57 g/cm^3, equivalent to approximately 93.3–98.1% of the calculated theoretical density. A major challenge associated with KNN-based ceramics is the evaporation of alkali metals (K^+, Na^+, Li^+) during high-temperature sintering, which disrupts the target stoichiometry and makes it difficult to achieve the optimal physical properties. To address this, the present study combined a two-step sintering technique with the co-doping of Bi^{3+} and Hf^{4+} ions. This approach stabilizes the KNN-based system at the sintering temperature, suppresses alkali metal evaporation, and ultimately enhances the macroscopic electrical properties. When a minor fraction of alkali metal ions evaporates, it creates favorable structural conditions for

Bi^{3+} to occupy *A*-site vacancies, yielding improved bulk densities up to 98.1%, consistent with the mechanism proposed by Naceur et al.[14]. Additionally, the incorporation of BNH into LKNNS ceramics effectively lowers the sintering temperature. This effect is attributed to the presence of Bi, which exhibits a relatively low melting point (just above 271 °C) and enhances densification, leading to higher crystallinity and microstructural refinement.

The XRD patterns of the $(1-x)$LKNNS– xBNH samples were measured over a 2q range for 20°–60°. All compositions exhibited a stable, single-phase perovskite structure in the range of x = 0–0.35. To further elucidate the detailed phase evolution, Rietveld refinement was performed on the diffraction data, as illustrated in Fig. 3. The corresponding refinement parameters are summarized in Table 1. The refinement model adequately reproduces the diffraction peak profiles, positions, structural features, and background. The low residual factors (R_{wp} and R_p) confirm the high quality of the fit and reveal a gradual transformation of the crystal symmetry as x increases. The crystal structure of the LKNNS−BNH ceramics systematically evolves with increasing BNH content. A composition-driven structural transition occurs from the host orthorhombic symmetry (*Amm*2, characterized by splitting of the $(022)_O$ and $(200)_O$ peaks) toward a rhombohedral phase (*R*3*m*, associated with the singlet $(200)_R$ reflection). Between these two states, a mixed *R*3*m*–*P*4*mm* phase region appears, confirmed by the characteristic splitting of the $(002)_T$ and $(200)_T$ peaks. Specifically, at x = 0, the pristine LKNNS ceramic exhibits a high *O* phase fraction of 80.15%, alongside a low *T* phase fraction of 19.85% (Table 1). However, as BNH is added, the *T* phase fraction increases markedly from 19.85% to 75.44%. As shown in Table 1, the *O* phase fraction continuously decreases with increasing x, dropping from 80.15% (x = 0.000) to 54.55% (x = 0.015), and becomes undetectable at x = 0.025. Conversely, an *R* phase emerges at x = 0.025, as evidenced by the appearance of the $(200)_R$ diffraction peak. The phase analysis confirms the formation of a dual-phase *T*–*R* state at x = 0.025, as supported by the refinement results shown in Fig. 3 and summarized in Table 1. From an ionic radius perspective, Hf^{+} (0.76 Å) possesses a similar size to Nb^{5+} (0.64 Å) and Sb^{5+} (0.62 Å), enabling its incorporation into the *B*-site of the perovskite framework, while remaining significantly smaller than the *A*-site cations, namely Li^{+}(0.92 Å), Na^{+} (1.32 Å), and K^{+} (1.38 Å). In contrast, the ionic radius of Bi^{3+}(1.03 Å) matches more closely with that of the A-site, substituting for Li^{+}, K^{+}, or Na^{+}. This balanced co-substitution maintains structural stability and supports the formation of a homogeneous solid solution[15,16].

Through XRD analysis, Tao et al.[13] demonstrated that the structural characteristics of $(1-x)$KNNS–xBNH ceramics evolved from an *O* phase to a *T* phase as x increased from 0 to 0.05, establishing a well-developed *R*–*T* phase boundary across the composition range of $0.04 \leq x \leq 0.08$. Similarly, Xie et al.[17] reported that $0.965\text{KNNS}-0.035[(Bi_{0.5}Na_{0.5})_{1-y}Co_yZrO_3]$ ceramics undergo a composition-driven phase evolution where the *O* structure progressively transforms into the *T* symmetry with increasing y, passing through a dual-phase *O*– *T* region within the narrow window of $0.03 \leq y \leq 0.045$.

The microstructure of $(1-x)$LKNNS– xBNH ceramics was determined from SEM images, as depicted in Fig. 4. All compositions exhibited well-developed microstructures characterized by uniform grain size, dense packing, and clearly defined grain boundaries. A gradual increase in grain size was noted with increasing x, reaching a maximum value of approximately 1.79 ± 0.12 μm at x = 0.035 (Fig. 5). The grain growth phenomenon can be explained by the diffusion of Bi and Hf from BNH into the LKNNS matrix. Because of their comparable ionic sizes, Hf^{+} (0.76 Å) is expected to substitute for Nb^{5+} and Sb^{5+} at the *B*-site, while Bi^{3+} (1.03 Å) preferentially replaces Li^{+}, K^{+}, or Na^{+} at the *A*-site[13]. These microstructural results are consistent with the bulk density measurements (Fig. 1). The improved densification and uniform grain structure observed in this work can be attributed to the two-step sintering process, which effectively suppresses abnormal grain growth while maintaining a high driving force for densification. According to our previous research on LKNNS ceramics[9], a denser microstructure with fewer pores and uniformly sized grains may be ascribed to the enhanced polarization efficiency caused by easy domain switching, resulting in improved electrical properties.

The room-temperature dielectric properties, specifically the ε_r and $\tan\delta$, of the $(1-x)$LKNNS–xBNH system at 10 kHz are plotted against x in Fig. 6. With increasing BNH concentration, ε_r exhibits a steady enhancement, reaching a maximum value of 1137 at x = 0.025. In contrast, $\tan\delta$ decreases to a minimum value of 0.040 at this composition. When x surpasses 0.025, a subsequent reduction in ε_r occurs alongside an increase in $\tan\delta$. Therefore, the composition with 0.025 BNH demonstrates superior dielectric performance relative to the other samples. Ullah et al.[18] attributed the enhancement in dielectric properties to

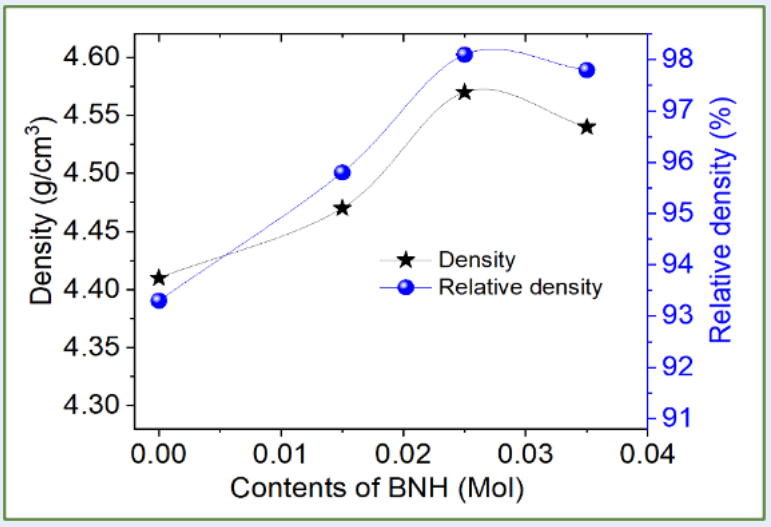

Figure 1: Density of (1−x)LKNNS–xBNH materials with varying x. [Source: Authors]

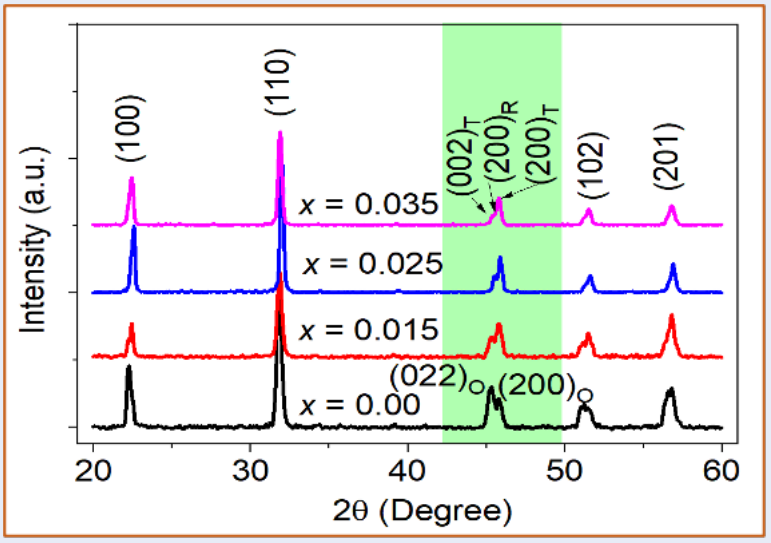

Figure 2: XRD patterns for (1−x)LKNNS–xBNH with varying x. [Source: Authors]

increased ceramic density, larger grain sizes, and improved microstructural characteristics. Furthermore, the 0.975LKNNS–0.025BNH ceramic (x = 0.025) displayed a dual-phase configuration comprising T and R symmetries, which may contribute to enhanced dielectric properties, consistent with the observations of Tao et al.[13]. Ultimately, the combination of large particle sizes and the coexistence of the T– R phase facilitates polarization owing to easy domain switching, supporting further optimization of the dielectric properties.

The temperature-dependent behavior of ε_r at 10 kHz is presented in Fig. 7 for (1−x)LKNNS–xBNH with varying x sintered at 1050 °C for 4 h. All $e(T)$ curves exhibit two distinct peaks: the low-temperature peak corresponds to the ferroelectric O– T transition, and the second peak at a higher temperature is associated with T_C[19,20]. Both T_{O-T} and T_C were observed to decrease with increasing x content. With increasing x, T_C declines from 364 to 318 °C. Simultaneously, T_{O-T} shifts downward from 110 °C at x = 0.0 to 60 °C at x = 0.035. This behavior is attributed to solid-solution effects induced by BNH incorpora-

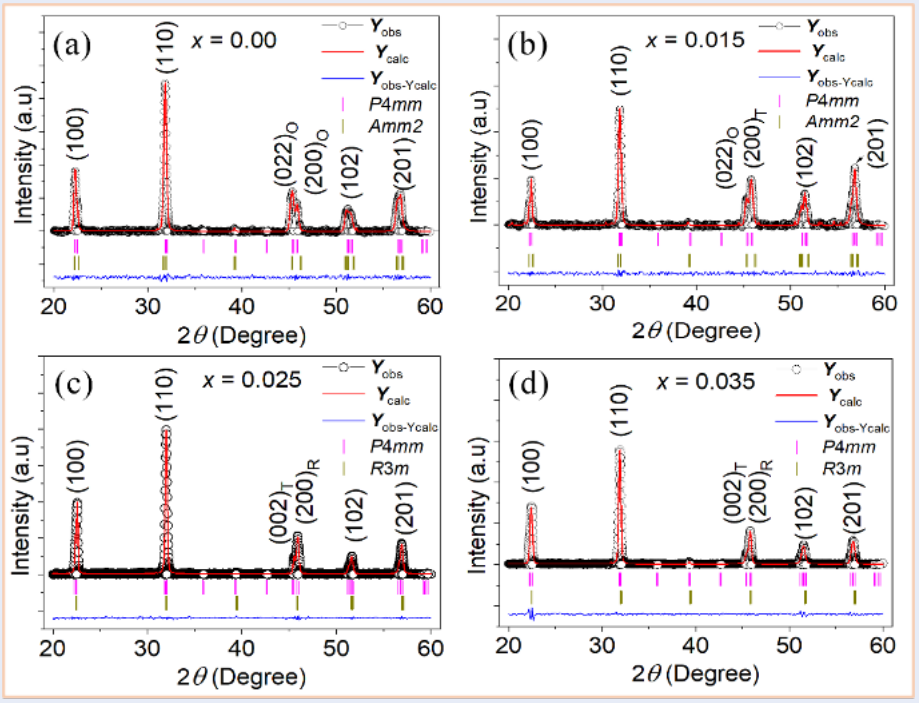

Figure 3: The XRD Rietveld refinement for (1−x)LKNNS–xBNH with varying x. [Source: Authors]

Table 1: Rietveld refinement datafor (1−x)LKNNS–xBNH as a function of composition. [Source: Authors]

Sample composition	Crystal symmetry	a (Å)	(Å)	c (Å)	V (Å3)	Phase fraction (%)	Rwp (%)	R (%)
x = 0.00	Amm2	3.9506	5.6462	5.6505	126.040	80.15	5.62	7.69
	4mm	3.9506	3.9506	4.0072	62.541	19.85		
x = 0.015	Amm2	3.9428	5.6363	5.6696	125.996	54.55	5.36	7.05
	4mm	3.9555	3.9555	4.0098	62.736	45.45		
x = 0.025	4mm	3.9534	3.9534	4.0085	62.649	75.44	5.90	7.89
	R3m	5.6021	5.6021	6.9320	188.406	24.56		
x = 0.035	4mm	3.9574	3.9574	3.9929	62.532	51.43	5.48	5.86
	R3m	5.6099	5.6099	6.8805	187.522	48.57		

tion. Specifically, Hf^{+} can enter the perovskite framework and replace *B*-site cations, whereas Bi^{3+} substitutes for *A*-site species[13]. The lower bond energy of Hf–O (530 kJ/mol) relative to Nb–O (771.5 kJ/mol) weakens the rigidity of the BO octahedral framework, thereby reducing the T_C[16]. As evidenced in Fig. 7(b), the peak dielectric constant (εx at T_C) increases progressively with BNH incorporation, attaining its highest value (6274) at x = 0.025 before diminishing at elevated concentrations. This dielectric improvement closely correlates with the change in piezoelectric properties, as discussed further in the following section. According to Li et al.[17] and Tu et al.[21], a dense microstructure with few pores, small grain boundaries, and the coexistence of the *T*--*O* phase results in improved dielectric properties due to easy domain switching under an electric field.

To elucidate the impact of BNH modification on relaxor characteristics, the logarithmic relationship between $(1/\varepsilon - 1/\varepsilon_x)$ and $(T - T_C)$ was examined

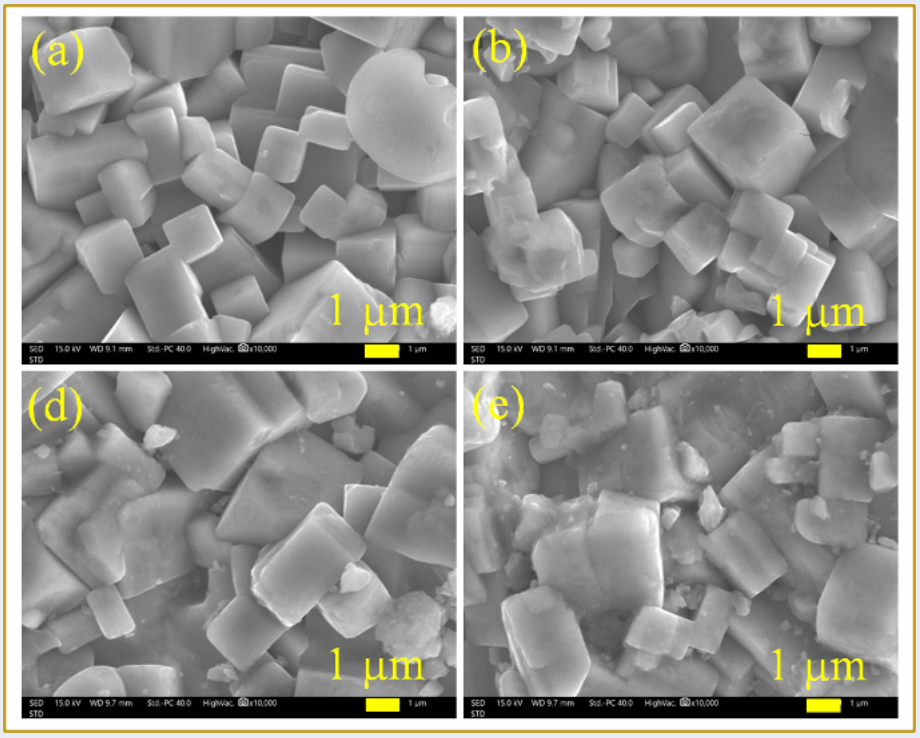

Figure 4: Microstructural features of(1−x)LKNNS–xBNH with varying x. [Source: Authors]

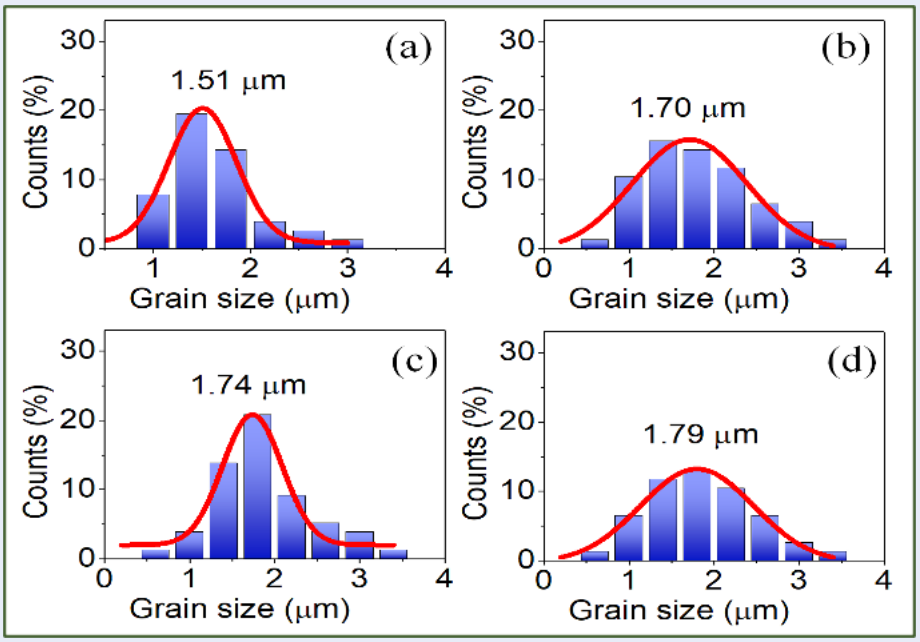

Figure 5: The grain size distributions of (1−x)LKNNS–xBNH with varying x. [Source: Authors]

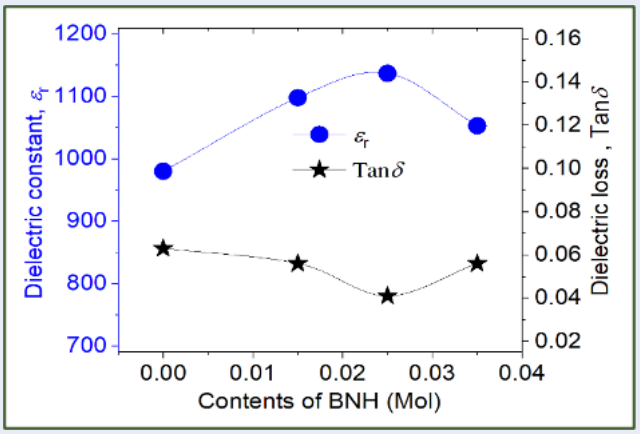

Figure 6: Relative permittivity (ε_r) and dielectric loss (tanδ) of (1−x)LKNNS–xBNH with varying x. [Source: Authors]

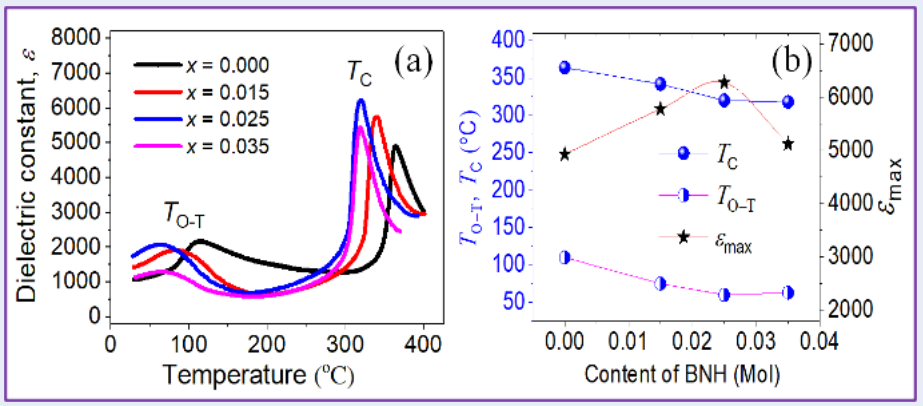

Figure 7: Temperature-dependent variation of the dielectric properties for (1−x)LKNNS–xBNH. [Source: Authors]

and plotted, as shown in Fig. 8 [22]. The diffuseness parameter (γ) values for (1−x)LKNNS− xBNH ceramics were determined to be 1.34, 1.37, 1.39, and 1.56 for x = 0.0, 0.015, 0.025, and 0.035, respectively. This may be explained by the substitution of Bi^{3+} and Hf^{4+} ions from BNH into the LKNNS matrix, replacing Li^+, Na^+, K^+, and Sb^{5+}, or Nb^{5+} ions [22–25]. Chen et al. [26] suggested that during the sintering process of KNN-based ceramics, a small number of alkali metal ions (K^+, Na^+, Li^+) evaporate, which creates favorable conditions for Bi^{3+} to occupy A-site vacancies and may cause A-site cation disorder, resulting in a diffuse phase transition. According to Li et al. [27], diffuse phase transition behavior can also be attributed to compositional variations affecting the stable positions of B-site cations when Hf^{4+} substitutes for Sb^{5+} or Nb^{5+}, which prompts the formation of polar nanoregions. Such heterovalent and size-mismatched substitutions introduce local structural disorder within the ABO_3 perovskite structure, leading to a more diffuse dielectric transition and an increase in γ values, which aligns with the observations reported by Tu et al. [21].

The inverse dielectric constant ($1/\varepsilon$) as a function of temperature for $T > T_B$ is depicted in Fig. 9 for the (1−x)LKNNS–xBNH compositions. Above the Burns temperature (T_B), the dielectric behavior conforms to the modified Curie–Weiss model, as confirmed by the linear fitting of the $1/\varepsilon$–T relationship in this temperature region. The derived fitting parameters are listed in Table 2. For the 0.975LKNNS–0.025BNH sample, T_{O-T} and T_C were approximately 60 and 320 °C, respectively. In addition, the characteristic temperatures T_o and T_B, together with the diffuseness parameter ΔT_m, were evaluated to be 286, 332, and 12 °C. These results are in close agreement with those reported by Tu et al. [21] for CuO-modified $(Na_{0.59}K_{0.41})(Nb_{0.4}Ta_{0.1}Sb_{0.0})O_3$ ceramics, where

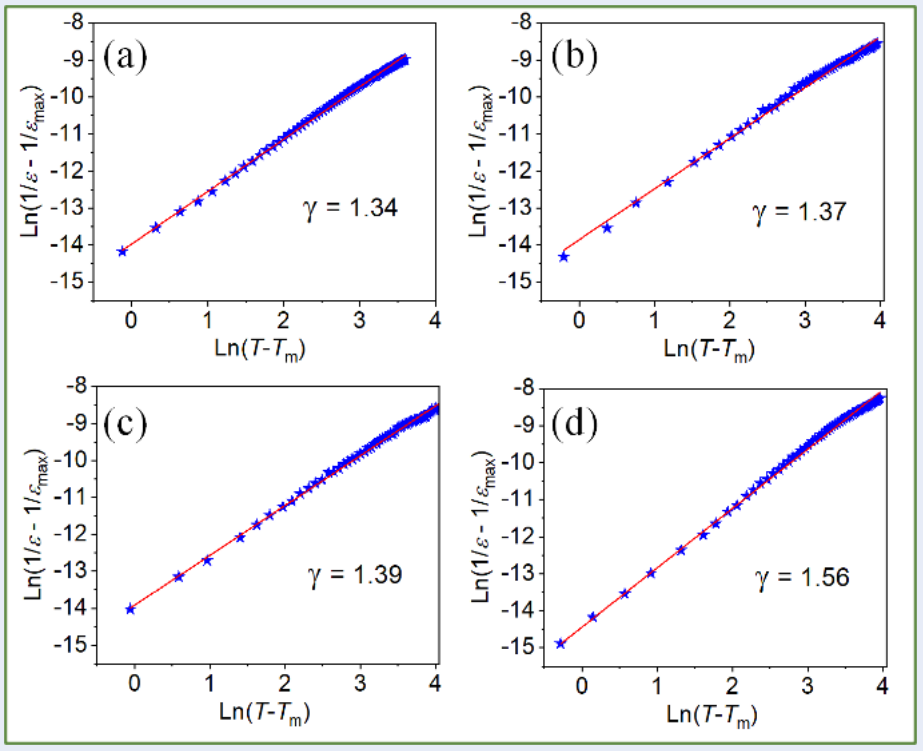

Figure 8: Diffuseness parameter of (1−x)LKNNS–xBNHwith varying x. [Source: Authors]

the characteristic temperatures T_{O-T}, T_o, T_C, and T_B were approximately 50, 323, 325, and 361 °C, respectively, with a diffuseness parameter ΔT_m of 36 °C. In comparison, the present 0.975LKNNS–0.025BNH composition exhibits a significantly smaller ΔT_m value (12 °C), indicating a weaker degree of relaxor behavior and a more diffuse-to-normal ferroelectric transition tendency. This difference may be associated with the relatively moderate compositional disorder introduced by Hf^{+} substitution at the *B*-site and Bi^{3+} incorporation at the *A*-site, which induces local lattice distortion but does not generate sufficiently strong random fields to produce pronounced relaxor characteristics. Consequently, the dielectric response of the present system retains a predominantly ferroelectric nature with limited diffuseness.

To further elucidate the electromechanical response, the room-temperature piezoelectric properties of the (1−*x*)LKNNS– *x*BNH ceramics ($0 \leq x \leq 0.035$) were systematically evaluated using the resonance–antiresonance method, as shown in Fig. 10. The resonant vibration spectra were employed to determine the key piezoelectric parameters, including d_{33} and k⊠, thereby stablishing a correlation among the compositional evolution, phase boundary characteristics, and electromechanical performance. Based on these spectra, the corresponding piezoelectric parameters of the ceramics were extracted, as presented in Fig. 11. Fig. 11 depicts the compositional dependence of k⊠, kt, and d_{33} for the (1−*x*)LKNNS–*x*BNH ceramics. Incorporation of BNH into the LKNNS matrix markedly enhanced the electromechanical performance. With increasing BNH concentration from x = 0.00 to 0.035, k⊠, kt, and d_{33} exhibited pronounced increases, attaining maximum values of 0.37, 0.39, and 230 pC/N at x = 0.025, respectively. Further BNH addition led to a gradual decline in these parameters. In contrast, the undoped LKNNS sample displayed substantially lower values (k⊠ = 0.33, kt = 0.36, and d_{33} = 145 pC/N). The superior piezoelectric response at x = 0.025 can be attributed to the optimized densification and refined microstructure achieved via the two-step sintering route, which facilitates domain wall motion and polarization switching. Furthermore, the enhancement in piezoelectric performance can be interpreted in terms of phase boundary engineering. Zhang et al.[12] demonstrated that 0.955KNNS–0.045BNH ceramics achieved an outstanding d_{33} value of 540 pC/N, which was attributed to the coexistence of *R*, *O*, and *T* phases. Similarly, Tao et al.[13] reported that compositions positioned near the *R*–*T* phase boundary, specifically

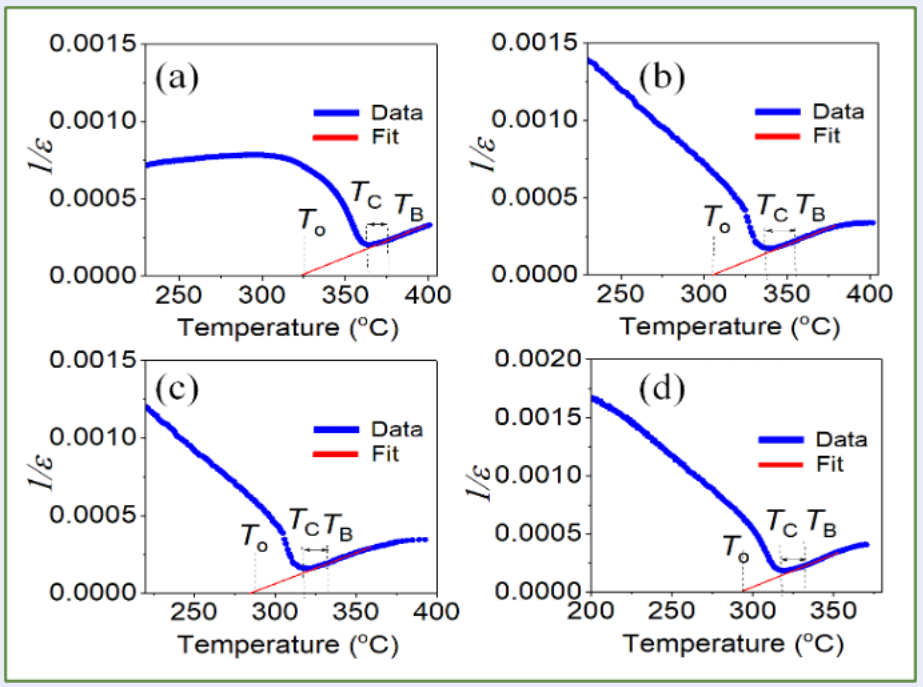

Figure 9: Temperature dependence of the inversedielectric constant (1/ε) for (1−x)LKNNS–xBNH. [Source: Authors]

Table 2: Relaxor characteristics of(1−x)LKNNS–xBNH with varying x. [Source: Authors]

Parameters	x = 0.00	x = 0.015	x = 0.025	x = 0.035
TO–T (°C)	110	75	60	63
TC (°C)	364	342	320	318
To (°C)	324	305	286	292
TB (°C)	375	354	332	332
DTm (°C)	11	12	12	14
γ	1.34	1.37	1.39	1.56

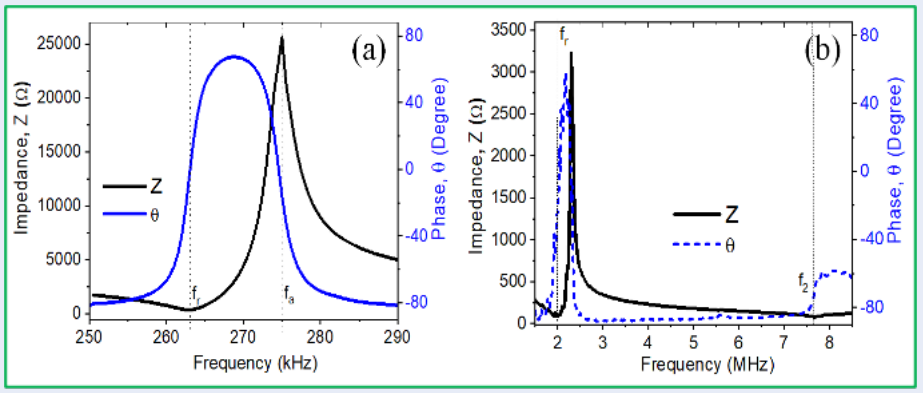

Figure 10: The resonance spectrum of 0.975LKNNS-0.025BNH: (a) Radial resonance spectrum; (b) Thickness resonance spectrum. [Source: Authors]

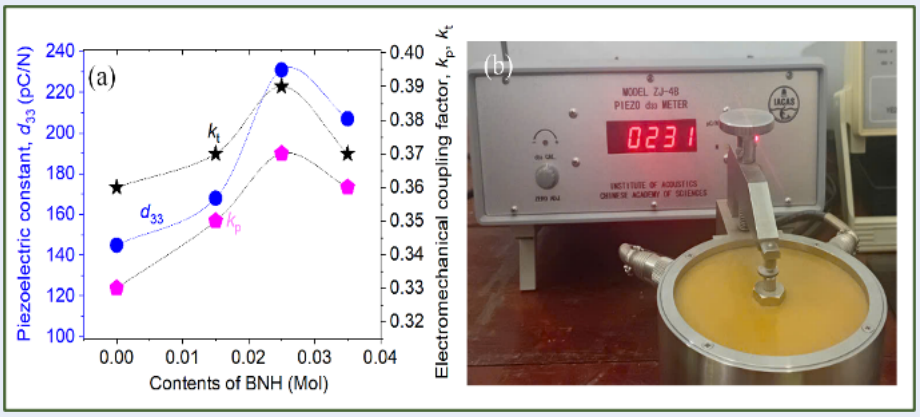

Figure 11: (a) The k_p,k_t, and d_{33} values of (1−x)LKNNS–xBNH with varying x; (b) Measured d_{33} value displayed on the piezo-d_{33} meter. [Source: Authors]

0.965KNNS–0.035BNH, exhibited a high d_{33} = 418 pC/N and an enhanced planar coupling factor (k ≈ 0.45). These improvements were likewise correlated with multiphase coexistence within the phase boundary region. Taken together, the simultaneous optimization of microstructural features—namely high densification and enlarged grain size—along with the formation of an *R*– *T* phase boundary, plays a decisive role in facilitating polarization rotation and domain wall motion, thereby leading to the observed enhancement in both the dielectric and piezoelectric responses.

The d_{33} values (~230 pC/N) in this study are lower than those reported previously, such as those by Zhang et al.[12] and Tao et al.[13], but this variance may be related to differences in defect chemistry, sinterability, and phase stability. As explained above, alkali metal evaporation can be mitigated by substituting Bi elements in the A-site vacancies[14], which suppresses abnormal grain growth while maintaining effective densification, resulting in high bulk densities of up to 4.57 g/cm^3 (98.1% relative density). The primary reason for the lower room-temperature piezoelectric properties compared with other published data[12,13] is the position of the phase transitions. Herein, the T_{O-T} value gradually decreased from 110 °C (x = 0.0) to 60 °C (x = 0.025, Fig. 7(b)), whereas the compositions optimized by Tao et al. shifted the phase transition temperature from 75 °C to room temperature (27 °C), as reported[13]. It is widely accepted that the peak piezoelectric properties are achieved in these systems when the *R* and *T* phases fully coexist at room temperature, thereby lowering the energy barrier for structural change and polarization rotation[28]. Nevertheless, the electrical and electrochemical properties obtained in this work remain highly competitive and viable for lead-free functional materials, making the proposed system suitable for practical applications in piezoelectric actuators, sensors, and energy harvesting devices.

The ferroelectric *P*–*E* hysteresis loops of the (1−*x*)LKNNS– *x*BNH ceramics are presented in Fig. 12(a), revealing well-defined ferroelectric characteristics for all compositions. From these loops, the remanent polarization (P_r) and coercive field (E_C) were determined and are summarized in Fig. 12(b). As the BNH content increased from x = 0.00 to 0.035, P_r exhibited an initial enhancement, reaching a maximum value of 15.6 μC/cm^2 at x = 0.015, followed by a gradual reduction at higher concentrations. In contrast, E_C decreased continuously with increasing BNH incorporation, indicating enhanced domain switching behavior upon compositional modification.

The improved ferroelectric response at x = 0.015 can be ascribed to the emergence of a compositional phase boundary between the *O* and *T* phases, which enhances polarization rotation and domain reorientation. As previously discussed, incorporation of Bi^{3+} and Hf^{4+} ions into the LKNNS lattice leads to a reduction in both T_C and T_{O-T}, while the *R*–*O* transition temperature progressively shifts toward room temperature. The resulting convergence of these phase transition temperatures favors the development of an *O*– *T* phase coexistence region near ambient conditions. This multiphase configuration facilitates domain wall mobility and polarization switching, thereby strengthening the ferroelectric properties, in agreement with the observations reported by Liu et al.[29].

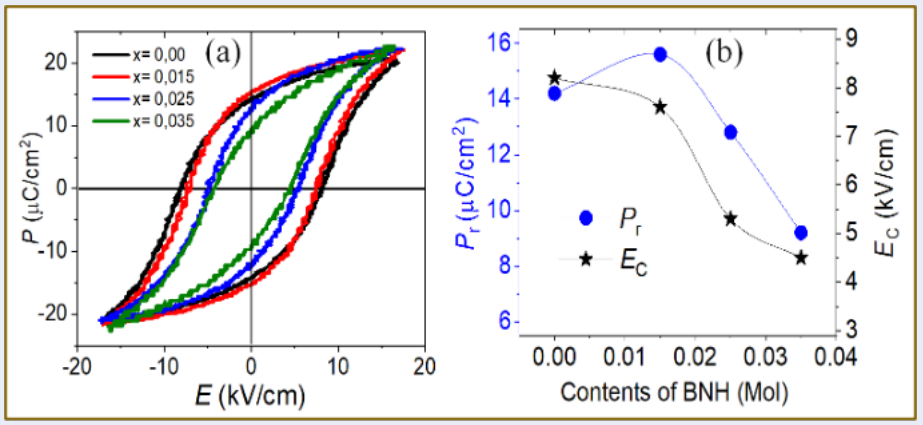

Figure 12: (a) P–E hysteresis loops; (b) Ferroelectric properties of (1−x)LKNNS–xBNH with varying x. [Source: Authors]

CONCLUSION

Lead-free (1−x)LKNNS–xBNH ceramics (x = 0.0–0.035) were successfully fabricated using phase structure modification combined with a two-step sintering technique. Structural analysis demonstrated that the incorporation of Bi^{3+} and Hf^{4+} into the LKNNS lattice induced a structural transformation from an *Amm*2 phase to a *R*3*m* phase through the coexistence of *R*3*m* and *P*4*mm* phases. This phase evolution effectively improved the physical properties of the LKNNS–BNH ceramics. At a doping level of 0.025 mol BNH, the ceramics exhibited beneficial overall electrical performance, specifically achieving k_t = 0.39, k = 0.37, d_{33} = 230 pC/N, ε_r = 1137, e_{max} = 6274, and tanδ = 0.04. Meanwhile, a relatively high $_r$ of 15.6 μC/cm^2 was achieved at x = 0.015, indicating a strong ferroelectric response. Additionally, the dielectric relaxation behavior of the 0.975LKNNS−0.025BNH ceramic was systematically investigated to determine key phase transition parameters, including T_{O-T} (60 °C), D T_m (12 °C), and g (1.39). These results demonstrate that LKNNS–BNH ceramics are promising candidates for practical applications, including piezoelectric actuators, sensors, and energy harvesting devices, maintaining reliable performance over a broad temperature range enabled by their high T_C (318–364 °C).

ACKNOWLEDGEMENT

This research is funded by Vietnam National Foundation for Science and Technology Development (NAFOSTED) under grant number 103.02-2023.13

AUTHOR'S CONTRIBUTIONS

Le Dai Vuong conceptualized the study and supervised the research. Vo Quang Nha and Huynh Thi Thuy Linh performed the experiments and material characterization. Le Van Tan contributed to data analysis, interpretation of results, and manuscript preparation. Vo Thanh Tung assisted in structural and electrical measurements. Vo Thi Thanh Kieu contributed to data validation and manuscript revision. All authors read and approved the final manuscript.

FUNDING

This research is funded by Vietnam National Foundation for Science and Technology Development (NAFOSTED) under grant number 103.02-2023.13

COMPETING INTERESTS

The authors declare that they have no competing interests.

REFERENCES

1. Vuong LD, Gio PD, Quang NDV, Hieu TD, Nam TP. Development of 0.8Pb(Zr0.48Ti0.52)O3–0.2Pb[(Zn1/3Nb2/3)0.625(Mn1/3Nb2/3)0.375]O3 Ceramics for High-Intensity Ultrasound Applications. Journal of Electronic Materials. 2018;47(10):5944–5951. Available from: https://doi.org/10.1007/s11664-018-6454-8.
2. Vuong LD, Thinh NV, On DV, Tung VT. Improved piezoelectric properties of the Fe2O3-modified 0.97PSLZT-(0.03-x)BMT-xPMS for high-power piezoelectric applications. Journal of Materials Science: Materials in Electronics. 2025;36(4):284. Available from: https://doi.org/10.1007/s10854-025-14278-0.
3. Li B, Xiong C, Cao X, Wei X, Qiu Y, Gao D. Temperature stability of multilayer symmetric KNN-based ceramics with continuous phase transitions. Applied Physics Letters. 2025;126(3). Available from: https://doi.org/10.1063/5.0247218.
4. On DV, Vuong LD, Chuong TV, Quang DA, Tung VT. Study on the synthesis and application of BaTiO3 nanospheres. International Journal of Materials Research. 2021;112(6):448–456. Available from: https://doi.org/10.1515/ijmr-2020-8054.

5. Vuong LD, Gio PD. Enhancement in dielectric, ferroelectric, and piezoelectric properties of BaTiO3-modified Bi0.5(Na0.4K0.1)TiO3 lead-free ceramics. Journal of Alloys and Compounds. 2020;817:152790. Available from: https://doi.org/10.1016/j.jallcom.2019.152790.
6. Tu LTU, Tho NT. Selection and optimization of Sb and Ta co-doped (K0.41Na0.59)(Nb1-x-ySbxTay)O3 lead-free ceramics. Journal of Materials Science: Materials in Electronics. 2023;34(10):917. Available from: https://doi.org/10.1007/s10854-023-10368-z.
7. Gio PD, Vuong LD, Tu LTU. Enhanced piezoelectric and energy storage performance of 0.96(K0.48Na0.48Li0.04)(Nb0.95Sb0.05)O3–0.04Bi0.5(Na0.82K0.18)0.5ZrO3 ceramics using two-step sintering method. Journal of Materials Science: Materials in Electronics. 2021;32(10):13738–13747. Available from: https://doi.org/10.1007/s10854-021-05951-1.
8. Vuong LD, Lich NQ, Cuong NX, Nha VQ, Nhat ND, Hieu LD, et al. Optimization of the calcination and two-step sintering temperatures of (K0.48Na0.48Li0.04)(Nb0.95Sb0.05)O3 ceramics. Materials Research Express. 2023;10(10):105701. Available from: https://doi.org/10.1088/2053-1591/acf191.
9. Gio PD, Vuong LD, Tu LTU. Enhanced piezoelectric and energy storage performance of 0.96(K0.48Na0.48Li0.04)(Nb0.95Sb0.05)O3–0.04Bi0.5(Na0.82K0.18)0.5ZrO3 ceramics using two-step sintering method. Journal of Materials Science: Materials in Electronics. 2021;32(10):13738–13747. Available from: https://doi.org/10.1007/s10854-021-05951-1.
10. Gio PD, Viet HQ, Vuong LD. Low-temperature sintering of 0.96(K0.5Na0.5)NbO3-0.04LiNbO3 lead-free piezoelectric ceramics modified with CuO. International Journal of Materials Research. 2018;109(11):1071–1076. Available from: https://doi.org/10.3139/146.111706.
11. Vuong LD, Cuong NX, Lich NQ, Nhat ND, Hieu LD, Nha VQ, et al. The effect of BaZrO3 content on the structure, microstructure, and electrical properties of (K, Na)NbO3-based lead-free ceramics. Applied Physics A. 2025;131(5):383. Available from: https://doi.org/10.1007/s00339-025-08517-8.
12. Zhang J, Sun X, Su W, Yao W, Zhou C. Superior piezoelectricity and rhombohedral-orthorhombic-tetragonal phase coexistence of (1-x)(K,Na)(Nb,Sb)O3-x(Bi,Na)HfO3 ceramics. Scripta Materialia. 2020;176:108–111. Available from: https://doi.org/10.1016/j.scriptamat.2019.09.017.
13. Tao H, Wu W, Wu J. Electrical properties of holmium doped (K,Na)(Nb,Sb)O3–(Bi,Na)HfO3 ceramics with wide sintering and poling temperature range. Journal of Alloys and Compounds. 2016;689:759–766. Available from: https://doi.org/10.1016/j.jallcom.2016.08.037.
14. Naceur H, Megriche A, Maaoui ME. Effect of sintering temperature on microstructure and electrical properties of Sr1-x(Na0.5Bi0.5)xBi2Nb2O9 solid solutions. Journal of Advanced Ceramics. 2014;3(1):17–30. Available from: https://doi.org/10.1007/s40145-014-0089-x.
15. Tu LTU, Vuong LD, Cuong NX, Lich NQ, Nhat ND, Hieu LD, et al. Improvement of the electrical properties of textured BNKT-modified (K, Na)NbO3 lead-free ceramics in the broad operating temperature range. Journal of Materials Science: Materials in Electronics. 2024;35(19):1363. Available from: https://doi.org/10.1007/s10854-024-13120-3.
16. Tu LTU, Vuong LD, Dat TN, Tung VT. Effects of CuO doping on the sintering behavior and piezoelectric properties of lead-free (K0.41Na0.59)(Nb0.84Sb0.06Ta0.10)O3 ceramics. Applied Physics A. 2025;131(3):210. Available from: https://doi.org/10.1007/s00339-025-08336-x.
17. Xie L, Xing J, Tan Z, Jiang L, Chen Q, Wu J, et al. Comprehensive investigation of structural and electrical properties of (Bi, Na) CoZrO3-doped KNN ceramics. Journal of Alloys and Compounds. 2018;758:14–24. Available from: https://doi.org/10.1016/j.jallcom.2018.05.102.
18. Dwivedi S, Pareek T, Kumar S. Structure, dielectric, and piezoelectric properties of K0.5Na0.5NbO3-based lead-free ceramics. RSC Advances. 2018;8(43):24286–24296. Available from: https://doi.org/10.1039/C8RA04038A.
19. Vuong LD, Quang DA, Tung VT, Chuc NH, Trac NN. Synthesis of textured Bi0.5(Na0.8K0.2)0.5TiO3–Ba0.844Ca0.156(Zr0.096Ti0.904)O3 lead-free ceramics for improving their electrical and energy storage properties. Journal of Materials Science: Materials in Electronics. 2020;31(20):18056–18069. Available from: https://doi.org/10.1007/s10854-020-04356-w.
20. Huang T, Xiao DQ, Liang WF, Wu JG, Wang Z, Zhu JG. Sintering Behavior of KNN-BNKT Lead-free Piezoelectric Ceramics. Ferroelectrics. 2014;458(1):37–42. Available from: https://doi.org/10.1080/00150193.2013.849978.
21. Ullah A, Ahn CW, Hussain A, Kim IW. The effects of sintering temperatures on dielectric, ferroelectric and electric field-induced strain of lead-free Bi0.5(Na0.78K0.22)0.5TiO3 piezoelectric ceramics synthesized by the sol–gel technique. Current Applied Physics. 2010;10(6):1367–1371. Available from: https://doi.org/10.1016/j.cap.2010.05.004.
22. Ghosh SK, Chauhan V, Hussain A, Rout SK. Phase transition and energy storage properties of BaTiO3-modified Bi0.5(Na0.8K0.2)0.5TiO3 ceramics. Ferroelectrics. 2017;517(1):97–103. Available from: https://doi.org/10.1080/00150193.2017.1370266.
23. Wang Y, Lu Y, Wu M, Wang D, Li Y, Wang Y. Phase Structure and Enhanced Piezoelectric Properties of Lead-Free Ceramics (1-x)(K0.48Na0.52)NbO3–(x/5.15)K2.9Li1.95Nb5.15O15.3 with High Curie Temperature. International Journal of Applied Ceramic Technology. 2012;9(1):221–227. Available from: https://doi.org/10.1111/j.1744-7402.2011.02650.x.
24. Zhai Y, Qi X, Tian G, Wang J, Yu F, Gai Z, et al. Improved energy-harvesting performance of (K, Na)NbO3-based ceramics through the synergistic effect of texture and defect engineering. Journal of the European Ceramic Society. 2025;45:116984. Available from: https://doi.org/10.1016/j.jeurceramsoc.2024.116984.
25. Vuong LD, Tho NT. The sintering behavior and physical properties of Li2CO3-doped Bi0.5(Na0.8K0.2)0.5TiO3 lead-free ceramics. International Journal of Materials Research. 2017;108(3):222–227. Available from: https://doi.org/10.3139/146.111465.
26. Rastogi SK, Divya P, Praveenkumar B, Kumar A. Effect of Sr2+, Ba2+ and Ta5+ ions on structural and electrical properties of BNKT ceramics. Materials Today: Proceedings. 2015;2:2784–2788. Available from: https://doi.org/10.1016/j.matpr.2015.07.277.
27. Eoh YJ, Kim ES. Effects of Ca2+ substitution on dielectric properties of (Ba0.7Sr0.3)(Ti0.9Zr0.1)O3 ceramics. Japanese Journal of Applied Physics. 2014;53(8S3):08–04. Available from: https://doi.org/10.7567/JJAP.53.08NB04.
28. Tu LTU, Vuong LD, Dat TN, Tung VT. Effects of CuO doping on the sintering behavior and piezoelectric properties of lead-free (K0.41Na0.59)(Nb0.84Sb0.06Ta0.10)O3 ceramics. Applied Physics A. 2025;131(3):210. Available from: https://doi.org/10.1007/s00339-025-08336-x.
29. Liu Y, Yi Y, Yu Y, Pan Y, He C, Liu X, et al. Microstructures, phase evolution and electrical properties of (1-x)K0.40Na0.60Nb0.96Sb0.04O3-xBi0.5K0.5HfO3 lead-free ceramics. Ceramics International. 2019;45(5):6328–6334. Available from: https://doi.org/10.1016/j.ceramint.2018.12.117.